Communication

Monitoring the Growth of Polyoxomolybdate Nanoparticles in Suspension by Flow Field-Flow Fractionation

Bailin Chen, Huijian Jiang, Yan Zhu, Arthur Cammers, and John P. Selegue

J. Am. Chem. Soc., **2005**, 127 (12), 4166-4167• DOI: 10.1021/ja045067r • Publication Date (Web): 03 March 2005

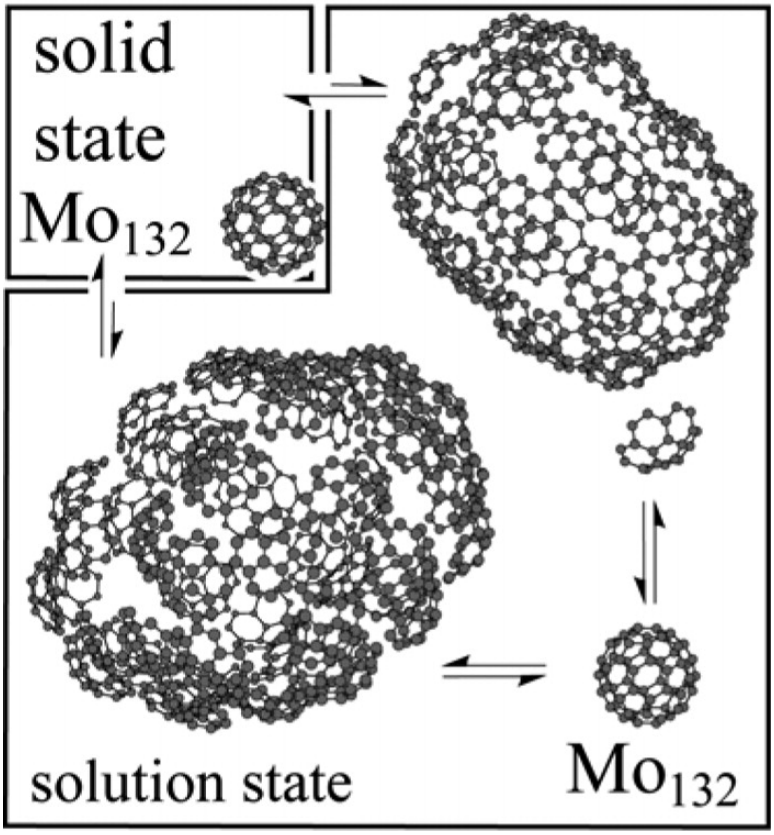

More About This Article

Additional resources and features associated with this article are available within the HTML version:

- Supporting Information
- Links to the 3 articles that cite this article, as of the time of this article download
- Access to high resolution figures

J|A|C|S
COMMUNICATIONS

Published on Web 03/03/2005

Monitoring the Growth of Polyoxomolybdate Nanoparticles in Suspension by Flow Field-Flow Fractionation

Bailin Chen, Huijian Jiang, Yan Zhu, Arthur Cammers, and John P. Selegue*

Department of Chemistry, University of Kentucky, Lexington, Kentucky 40506

Received August 16, 2004; E-mail: selegue@uky.edu

Reduction reactions of molybdate in acidic, aqueous solution lead to colored, mixed-valent $Mo^{V/VI}$ polyoxomolybdate (POM) species.[1−5] The two-century-old mystery of the "molybdenum blues"[6] exemplifies the difficulty in characterizing suspensions of POM particles. Müller, Liu, and co-workers revealed the fundamental compositions of the related "molybdenum browns", including I_h symmetrical keplerates. In general, reduced molybdates assemble into nanometric species (Figure 1a). Light-scattering, small-angle X-ray scattering (SAXS), and microscopy show slow aggregation of $Na_{15}[Mo^{VI}_{126}Mo^{V}_{28}O_{462}H_{14}(H_2O)_{70}]_{0.5}$-$[Mo^{VI}_{124}Mo^{V}_{28}O_{457}H_{14}(H_2O)_{68}]_{0.5}$·ca.· 400 H_2O.[7,8] and neutral $[\{(Mo^{VI}(Mo^{VI}_5O_{21})(H_2O)_6\}_{12}\{Fe^{III}(H_2O)_6\}_{30}]$· ca.·150 H_2O.[9,10] Formation of POM nanostructures in the presence of polymers and surfactants has also been reported.[11−14] We report here a combination of physical methods that allows us to monitor the dynamics of the size distribution and the chemical nature of suspended POM particles derived from $\{Mo_{132}\}$ keplerate in situ.

The $\{Mo_{132}\}$ system is well suited for this investigation. Partial reduction of $(NH_4)_6Mo_7O_{24}$·$4H_2O$ with N_2H_4·H_2SO_4 in CH_3CO_2-NH_4/CH_3CO_2H buffer produces crystals of $(NH_4)_{42}[Mo^{VI}_{72}Mo^{V}_{60}O_{372}(CH_3CO_2)_{30}(H_2O)_{72}]$·ca.·$300H_2O$·ca.·10 $CH_3CO_2NH_4$. The $\{Mo_{132}\}$ keplerate anion is I_h symmetrical with charge −42 and diameter ca. 2.9 nm.[5,15,16] Light-scattering methods are hindered by the deep color of the $\{Mo_{132}\}$ suspension, although Liu and co-workers were able to use scattering methods to study aggregation in lighter colored[10,14,17] $\{Mo_{154}\}$[8] and MoO_3/triblock copolymers.[12,13] Although Müller and co-workers have studied surfactant-encapsulated $\{Mo_{132}\}$[11] and oxidized $\{Mo_{132}\}$ species[18,19] and Cammers et al. have kinetically coprecipitated $\{Mo_{132}\}$ with tripodal hexamine-triscrown ethers,[20] the evolution of nanometer species of an unperturbed $\{Mo_{132}\}$-derived suspension is uninvestigated.

The key methodology of our study is field-flow fractionation (FFF), a flow-based, chromatography-like separation and sizing technique that can monitor changes in the particle-size distribution of a suspension in situ. FFF is conducted in a thin, empty channel, with separation based on relative hydrodynamic behavior.[21−23] In flow field-flow fractionation (FlFFF), a cross-flow perpendicular to the direction of laminar channel flow forces dissimilar particles to different levels in the channel, where they are eluted at different flow velocities. FlFFF fractionates particles between 1 and 1000 nm and allows analysis of the eluate.[24]

We used FlFFF to monitor the evolution of molybdate nanoparticles in a $\{Mo_{132}\}$ suspension prepared by Müller's procedure.[7,15,16] Under our FlFFF conditions,[25] soluble species and particles smaller than 3 nm are swept to the waste stream by the cross-flow, while larger particles are separated and eluted through a UV−visible detector. FlFFF fractograms monitoring the absorbance of the eluate at 455 nm are shown in Figure 1b.

The particle-size distributions calculated[26] from the data in Figure 1b have diameters ranging from 3 to 75 nm, roughly distributed in three populations with maxima about 3.4, 12, and 25 nm. The mean diameter is 31(±1) nm (confidence level 95%), averaged over 24 FFF runs from 8 days. The baseline fractogram at 10 min indicates that no particles over ca. 3 nm had yet formed. At 2 h, the 3.4-nm population is largest. The total area under the fractogram increases rapidly from 2 to 8 h, at which time the 12- and 25-nm populations are larger. We suggest that the 3.4-nm particles, decreasing after 2 h but observed consistently throughout the entire period, are the $\{Mo_{132}\}$ with their associated counterions and solvation shell. The overall particle population reaches a maximum at ca. 8 h, decreases rapidly for about 2 days and more slowly thereafter (Figure 1b). The decrease parallels the precipitation of large particles that are not sampled by FlFFF shown in the SEM[27] image in Figure 2a. The precipitate is in dynamic equilibrium with species still in solution or suspension, yielding after several days ca. 0.1-mm octahedral crystals of $\{Mo_{132}\}$, $Fm\bar{3}$ with $a \approx 46$ Å,[15] shown in Figure 2b.

The particle-size distribution of the molybdate suspension was corroborated by AFM, SEM, and HRTEM. Good agreement between particle-size distributions obtained by FFF and microscopy suggests that the POM superstructures are stable to FlFFF channel- and cross-flows, isolation and storage in air, and vacuum treatment in the electron microscopes. In other experiments, we established that the size distribution is unchanged by dilution or the presence of Triton X-100 surfactant. AFM images[28] display roughly spherical particles in the 20−35 nm size range and agglomerates of these particles. Figure 2c shows a typical HRTEM[29] image of $\{Mo_{132}\}$-derived particles after 1 day. Measurement of about 400 particles on several HRTEM images gives a range from 4 to 80 nm diameter with mean 34(±2) nm (confidence level 95%). Figure 2c reveals the hollow nature of the POM nanostructures. Each particle consists of a darker ring surrounding a circle of nearly uniform intensity, consistent with a shell of POM building blocks surrounding an empty core. As discussed by Cammers et al,[20] a solid, spherical particle would be darker at the center. Diffraction "shadows", inferring highly ordered packing, are apparent in the upper right of the micrograph. Unfortunately, the nanoparticle concentration in the eluate is too dilute to view them directly by TEM or AFM, especially in the presence of the relatively high concentration of Triton X-100. Absorption at 455 nm in the UV/visible spectra of collected FFF fractions suggests that the nanoparticles consist of $\{Mo_{132}\}$ units or chemically similar species. Müller and Liu have suggested similar superstructures in suspensions of related $\{Mo_{154}\}$[7,8] and $\{Mo_{72}Fe_{30}\}$[10,14,17]

In a $\{Mo_{132}\}$ suspension, molybdenum can end up in three different forms: (1) suspended particles larger than 3 nm, which are eluted through the FlFFF detector; (2) soluble species and suspended particles smaller than 3 nm, which are removed by the cross-flow[25] and do not pass through the FlFFF detector; (3) precipitate, which is not sampled for FlFFF. Measuring the Mo content of FlFFF eluate fractions by ICP-OES[30] provides an independent, quantitative assay of the molybdenum distribution. Figure 1c compares Mo content in the suspension estimated by

10.1021/ja045067r CCC: $30.25

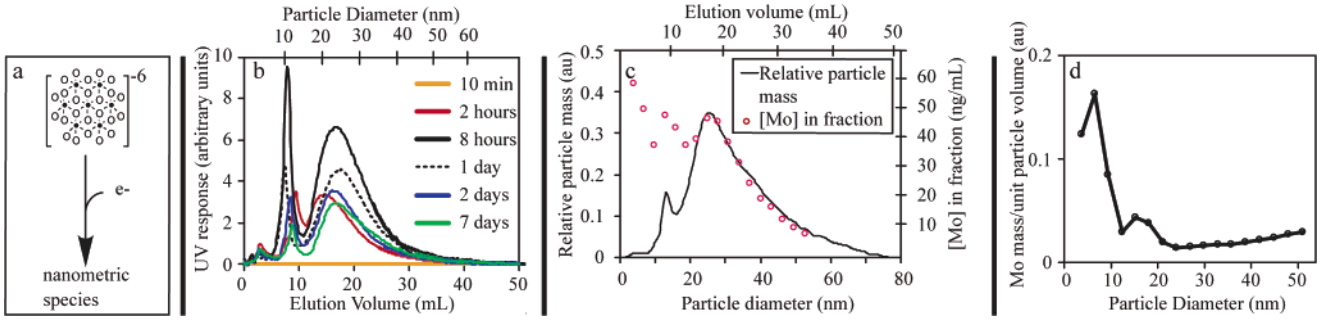

Figure 1. (a) Partial reduction of $[Mo_7O_{24}]^{6-}$ (b) Fractograms of $\{Mo_{132}\}$ nanoparticle growth over 7 days. (c) Mo content from summed area of FlFFF fractograms (relative particle mass) vs ICP-OES of eluent ([Mo] in fraction) on day 3. (d) Mo content per unit particle volume on day 3.

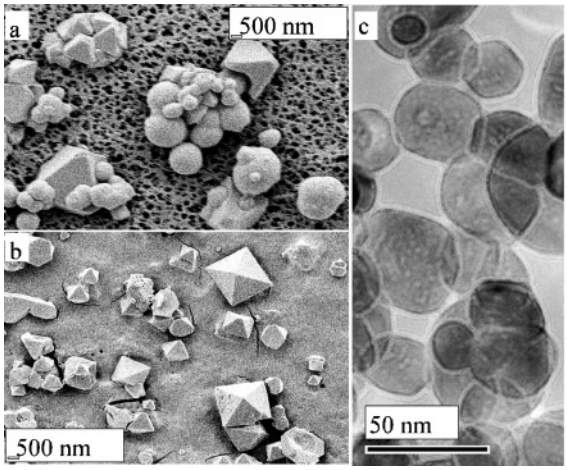

Figure 2. SEM image of POM precipitate after (a) 1 day, (b) 36 days, (c) HRTEM image of POM particles after 1 day.

summing the total area of FlFFF fractograms (expressed as "relative particle mass", assuming that the mass concentration of particles in the eluate is proportional to the UV detector signal and the particles have a constant density) vs the ICP-OES of eluate. The Mo distribution across a fractogram taken on day 3 is shown in Figure 1c. Above 25 nm in diameter, the FlFFF and ICP-OES curves are closely parallel. Below 25 nm in diameter, there is a secondary peak at 12 nm, and the Mo content by ICP-OES is much higher than by FlFFF. The discrepancy vanishes if abundant molybdate particles smaller than 25 nm do *not* have the keplerate-like structure of the larger particles, absorbing less strongly at 455 nm. The UV/visible spectra of a set of FlFFF fractions after day 3 (not shown) support this view. Although all fractions have a strong absorption at 455 nm, the strong absorption at 325 nm of the 3−5- and 9−11-nm fractions signals a different molybdate species. $[Mo^{VI}_6O_{19}]^{2-}$ has λ_{max} at 325 nm,[31] suggesting that the smaller particles have a higher Mo^{VI}/Mo^{V} ratio than the larger particles. Figure 1d shows the variation of Mo content per unit particle volume distribution vs particle size. The higher Mo content for particles below about 10 nm may be explained by small, Mo^{VI}-rich particles that form amorphous, non-keplerate aggregates. Upon further reduction and agglomeration, a particle eventually accumulates a critical number of POM building blocks, at which point it can organize into a 25-nm vesicle. The slight increase in Mo composition per unit particle volume with increasing particle size from 25 to 50 nm may indicate that the walls of larger vesicles can be thicker than a single layer.

Overall, this study shows the power of FlFFF combined with other techniques to investigate the dynamics of POM growth from small, amorphous particles to macroscopic crystals of $\{Mo_{132}\}$.

Acknowledgment. We acknowledge Dr. Alan Dozier for EM, and funds from U.S. DOE (DE-FG0200ER45847, subcontract 10186-00-23) and NSF (CHE0111578 and MRSEC DMR-9809686).

References

(1) Pope, M. T. Isopolyanions and heteropolyanions. In *Comprehensive Coordination Chemistry*; Wilkinson, G., Gillard, R. D., McCleverty, J. A., Eds.; Pergamon Press: Oxford, 1987; Vol. 3, pp 1023−1058.
(2) Pope, M. T. Polyoxo anions: synthesis and structure. In *Comprehensive Coordination Chemistry II*; McCleverty, J. A., Meyer, T. J., Eds.; Pergamon Press: Oxford, 2004; Vol. 4, pp 635−678.
(3) Müller, A.; Kogerler, P.; Kuhlmann, C. *Chem. Commun.* **1999**, 1347−1358.
(4) Cronin, L.; Kogerler, P.; Müller, A. *J. Solid State Chem.* **2000**, *152*, 57−67.
(5) Müller, A.; Koegerler, P.; Dress, A. W. M. *Coord. Chem. Rev.* **2001**, *222*, 193-218.
(6) Müller, A.; Serain, C. *Acc. Chem. Res.* **2000**, *33*, 2−10.
(7) Müller, A.; Diemann, E.; Kuhlmann, C.; Eimer, W.; Serain, C.; Tak, T.; Knoechel, A.; Pranzas, P. K. *Chem. Commun.* **2001**, 1928−1929.
(8) Liu, T.; Diemann, E.; Li, H.; Dress, A. W. M.; Müller, A. *Nature (London)* **2003**, *426*, 59−62.
(9) Müller, A.; Sarkar, S.; Shah, S. Q. N.; Bogge, H.; Schmidtmann, M.; Sarkar, S.; Kogerler, P.; Hauptfleisch, B.; Trautwein, A. X.; Schunemann, V. *Angew. Chem., Int. Ed.* **1999**, *38*, 3238−3241.
(10) Liu, T. *J. Am. Chem. Soc.* **2003**, *125*, 312−313.
(11) Volkmer, D.; Du Chesne, A.; Kurth, D. G.; Schnablegger, H.; Lehmann, P.; Koop, M. J.; Müller, A. *J. Am. Chem. Soc.* **2000**, *122*, 1995−1998.
(12) Liu, T.; Xie, Y.; Chu, B. *Langmuir* **2000**, *16*, 9015−9022.
(13) Liu, T.; Wan, Q.; Xie, Y.; Burger, C.; Liu, L.-Z.; Chu, B. *J. Am. Chem. Soc.* **2001**, *123*, 10966−10972.
(14) Liu, T. *J. Cluster Sci.* **2003**, *14*, 215−226.
(15) Müller, A.; Krickemeyer, E.; Bogge, H.; Schmidtmann, M.; Peters, F. *Angew. Chem., Int. Ed.* **1998**, *37*, 3360−3363.
(16) Cronin, L.; Diemann, E.; Müller, A. 4.27 Polyoxomolybdate Clusters: Nanoscopic Wheels and Balls. In *Inorganic Experiments*, 2nd ed.; Woollins, J. D., Ed.; Wiley-VCH: Weinheim, 2003; 340−346.
(17) Liu, T. *J. Am. Chem. Soc.* **2002**, *124*, 10942−10943.
(18) Müller, A.; Polarz, S.; Das, S. K.; Krickemeyer, E.; Bogge, H.; Schmidtmann, M.; Hauptfleisch, B. *Angew. Chem., Int. Ed.* **1999**, *38*, 3241−3245.
(19) Müller, A.; Shah, S. Q. N.; Bogge, H.; Schmidtmann, M.; Kogerler, P.; Hauptfleisch, B.; Leiding, S.; Wittler, K. *Angew. Chem., Int. Ed.* **2000**, *39*, 1614−1616.
(20) Zhu, Y.; Cammers-Goodwin, A.; Zhao, B.; Dozier, A.; Dickey, E. C. *Chem.—Eur. J.* **2004**, *10*, 2421−2427.
(21) Giddings, J. C. *Anal. Chem.* **1981**, *53*, 1170A−1172A, 1174A, 1176A, 1178A.
(22) Giddings, J. C. *Science* **1993**, *260*, 1456−65.
(23) Giddings, J. C. *Anal. Chem.* **1995**, *67*, 592A−598A.
(24) Schimpf, M. E.; Caldwell, K.; Giddings, J. C. *Field-Flow Fractionation Handbook*; Wiley-Interscience: New York, 2000; p 592.
(25) FFFractionation LLC Universal Fractionator model F1000, carrier liquid Milli-Q water containing 0.007% (w/v) Triton X-100 and 0.02% (w/v) NaN_3, channel flow 0.50 mL/min, cross-flow 3.00 mL/min, regenerated cellulose membrane with 10 000 amu (~2.2 nm) cutoff, detector at 455 nm, no light-scattering correction.
(26) Postnova analytics, version 2.0; FFF Analysis software.
(27) Hitachi S900 field-emission SEM.
(28) Digital Instruments NanoScope IIIa, glass substrate.
(29) JEOL 2010F field-emission TEM.
(30) Varian Vista-Pro CCD, Mo detection at 396.152 nm.
(31) Allcock, H. R.; Bissell, E. C.; Shawl, E. T. *Inorg. Chem.* **1973**, *12*, 2963−2968.

JA045067R